Ferrocene-Based Tris(1-pyrazolyl)borates: A New Approach to Heterooligometallic Complexes and Organometallic Polymers Containing Transition Metal Atoms in the Backbone

Fabrizia Fabrizi de Biani,[†] Frieder Jäkle,[‡] Michael Spiegler,[‡] Matthias Wagner,*[,‡] and Piero Zanello[†]

Anorganisch-chemisches Institut der Technischen Universität München, Lichtenbergstrasse 4, D-85747 Garching, Germany, and Universita di Siena, Dipartimento di Chimica, Pian dei Mantellini 44, 53100 Siena, Italy

Received October 10, 1996[⊗]

Starting from mono- and bifunctional ferrocene-based tris(1-pyrazolyl)borates, a novel route to oligonuclear complexes is presented, which incorporates transition metal centers differing substantially in their chemical nature. Both binuclear organometallics $FcB(pz)_3ML_n$ (Fc: ferrocenyl. pz: 1-pyrazolyl. ML_n: Tl, **1-Tl**; $Mo(CO)_3Li$, **1-MoLi**; $Mo(CO)_2(\eta^3$-methylallyl), **1-Mo**; $ZrCl_3$, **1-Zr**) and trinuclear complexes 1,1′-fc$[B(pz)_3ML_n]_2$ (fc: ferrocenylene. ML_n: Tl, **2-Tl**; $Mo(CO)_3Li$, **2-MoLi**; $Mo(CO)_2(\eta^3$-methylallyl), **2-Mo**) have been prepared. The trinuclear compound $[FcB(4\text{-}SiMe_3pz)_3]_2Fe$, **1-FeSi**, has been investigated as a model system for organometallic coordination polymers, consisting of the bifunctional linker 1,1′-fc$[B(pz)_3]_2^{2-}$ and transition metal ions M^{n+}. X-ray crystallography shows **1-Tl** to establish a polymeric structure in the solid state, while **1-Mo** features the usual tridentate coordination mode of the scorpionate ligand ($C_{25}H_{25}BFeMoN_6O_2$; $a = 8.756(1)$ Å, $b = 12.154(1)$ Å, $c = 12.927(1)$ Å, $\alpha = 105.26(1)°$, $\beta = 102.29(1)°$, $\gamma = 105.09(1)°$; triclinic space group $P\bar{1}$; $Z = 2$). With the exception of **1,2-Tl**, the anodic oxidation of the ferrocene moiety is generally reversible; cyclic voltammetry measurements indicate the two Mo centers in **2-Mo** and the two Fc moieties in **1-FeSi** to be noncommunicating.

Introduction

Since their invention in 1966,[1] tris(1-pyrazolyl)borates (scorpionates) have found widespread use as ligands in coordination chemistry.[2] The huge number of pyrazole derivatives known in the literature, together with the straightforward assembly of the tris(1-pyrazolyl)borate skeleton, offers a multiplicity of options for tailoring the access space to a metal held by the ligand,[3] as well as to influence the environment of a transition metal electronically.[2] Given this background and considering the fact that polynuclear transition metal complexes are of great current interest, it is surprising to see that only one derivative of the scorpionates bearing more than one tris(1-pyrazolyl)borate functionality has been described in the literature up to now (**A**).[4] The same is true for the rapidly growing field of redox-active ligands, where the only representative of poly(1-pyrazolyl)-borates is the ferrocene derivative **B** (Figure 1).[5]

Therefore, we got interested in the design and synthesis of a novel type of tris(1-pyrazolyl)borate **C**, where the ligand functionalities are grouped around the cylindrical redox-active ferrocene core. Ferrocene is ideally suited to serve as a backbone for this type of multifunctional ligands, because it can easily be borylated up to four times,[6−9] shows a reversible one electron oxidation, and provides a relatively rigid molecular framework. On the other hand, mutual rotation of both cyclopentadienyl rings enables those scorpionate complexes bound to different C_5H_4 units to come closer or to stay further apart. This rotational freedom should allow varying degrees of interaction between the transition metal centers and may thus give interesting cooperative effects, governed, for example, by changes in electronic charge. Henceforth, individual compounds of the general formula **C** are denoted **1**−**4**, depending on the number of ligand functionalities attached to the ferrocene core (Figure 2); the abbreviation Fc will be used for the monosubstituted ferrocenyl unit $(C_5H_5)Fe(C_5H_4)$, while fc stands for the 1,1′-disubstituted moiety $(C_5H_4)Fe(C_5H_4)$.

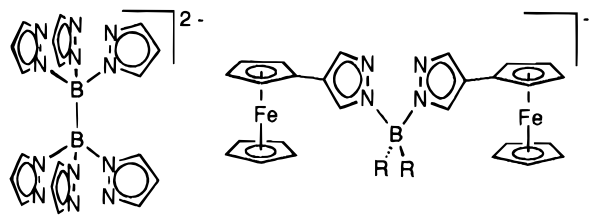

Figure 1. The only bifunctional tris(1-pyrazolyl)borate (**A**) and the only redox-active poly(1-pyrazolyl)borate (**B**) known today.

High-yield syntheses of ligands **1** and **2** have recently been reported by our group.[10] The thallium(I) derivative of the

[†] Universita di Siena. Telefax: (internat.) +39-577-280405. E-mail: (internat.) zanello@unisi.it.

[‡] Technische Universität München. Telefax: (internat.) +49-89-28913473. E-mail: (internat.) wagner@arthur.anorg.chemie.tu-muenchen.de.

[⊗] Abstract published in *Advance ACS Abstracts,* April 1, 1997.

(1) Trofimenko, S. *J. Am. Chem. Soc.* **1966**, *88*, 1842−1844.
(2) Trofimenko, S. *Chem. Rev.* **1993**, *93*, 943−980.
(3) Trofimenko, S.; Calabrese, J. C.; Thompson, J. S. *Inorg. Chem.* **1987**, *26*, 1507−1514.
(4) Brock, C. P.; Das, M. K.; Minton, R. P.; Niedenzu, K. *J. Am. Chem. Soc.* **1988**, *110*, 817−822.
(5) Niedenzu, K.; Serwatowski, J.; Trofimenko, S. *Inorg. Chem.* **1991**, *30*, 524−527.
(6) Ruf, W.; Fueller, M.; Siebert, W. *J. Organomet. Chem.* **1974**, *64*, C45−C47.
(7) Ruf, W.; Renk, T.; Siebert, W. *Z. Naturforsch.* **1976**, *31b*, 1028−1034.
(8) Wrackmeyer, B.; Dörfler, U.; Herberhold, M. *Z. Naturforsch.* **1993**, *48b*, 121−123.
(9) Appel, A.; Nöth, H.; Schmidt, M. *Chem. Ber.* **1995**, *128*, 621−626.
(10) Jäkle, F.; Polborn, K.; Wagner, M. *Chem. Ber.* **1996**, *129*, 603−606.

S0020-1669(96)01236-0 CCC: $14.00

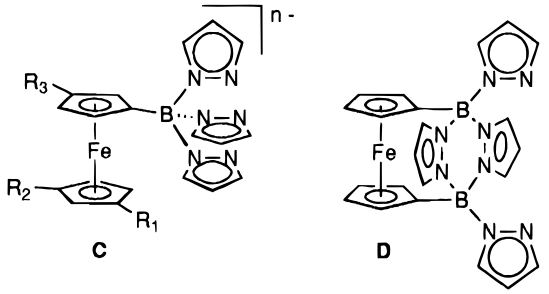

1 : R_1, R_2, R_3 = H ; n = 1

2 : R_1 = Bpz_3 ; R_2, R_3 = H ; n = 2

3 : R_1, R_2 = Bpz_3 ; R_3 = H ; n = 3

4 : R_1, R_2, R_3 = Bpz_3 ; n = 4

Figure 2. Multifunctional ferrocene-based tris(1-pyrazolyl)borates **C** and the pyrazabole-bridged ferrocenophane **D**.

monoscorpionate, **1-Tl**, provided the first example of a tris(1-pyrazolyl)borate complex adopting a polymeric structure in the crystal lattice. In this respect, **1-Tl** is very similar to thallium(I) cyclopentadienide, which establishes a zigzag polymer in the solid state.[11,12] The "free acid" **1-H** can also be generated without problems, and in the case of the discorpionate **2**, both the lithium salt and the Tl(I) complex (**2-Li**, **2-Tl**) are very stable compounds, which serve as useful starting materials for transition metal complexes. **2-H**, however, could not be obtained from 1,1′-bis(dibromoboryl)ferrocene and pyrazole (6 equiv)/NEt_3 (4 equiv). This reaction led to the formation of the respective *ansa*-ferrocene **D** (Figure 2).[10,13−15]

We have chosen the tris(1-pyrazolyl)borate moiety as a linker for the assembly of organometallic oligomers mainly because it offers much more convenient access to the desired compounds than the usual route by employing fulvalene- (and related) bridged heterooligometallics. Scorpionates have frequently been used as a substitute for cyclopentadienyl ligands η^5-C_5R_5, forming complexes which often demonstrate properties similar to their cyclopentadienyl counterparts.[2] To test whether this also holds for oligonuclear organometallics, we will compare the metal complexes of **C** with their metallocene analogs, whenever appropriate. Special emphasis will be given to the ligand properties of **1** and **2** toward a selection of metal centers of varying Lewis acidity (i.e. Zr(IV), Mo(II), Mo(0), Tl(I)), the type of denticity the tris(1-pyrazolyl)borate units will exhibit, and the consequences of complex formation on the redox behavior of the ferrocene backbone. In this context it is of interest to establish whether or not the ligand field strength of **1** and **2** can be influenced by changing the oxidation state of the ligand's iron atom, i.e. whether there is an electronic communication between the ferrocenyl substituent and the metal center bound to the scorpionate ligand. In general, metal−metal interaction in oligomeric complexes of **C** is a major topic of this paper.

Results and Discussion

Synthesis of $FcB(pz)_3ML_n$ and 1,1′-fc[$B(pz)_3ML_n$]$_2$. Lithium salts of the air-sensitive anions $FcB(pz)_3Mo(CO)_3^-$, **1-MoLi**, and 1,1′-fc[$B(pz)_3Mo(CO)_3]_2^{2-}$, **2-MoLi**, are synthesized by refluxing the respective scorpionate ligands **1-Li** and **2-Li** with excess $Mo(CO)_6$ in acetonitrile (pz = 1-pyrazolyl; Schemes 1 and 2).[16]

Scheme 1. Synthesis of Complexes **1-M** with Monofunctional Scorpionate Ligands[a]

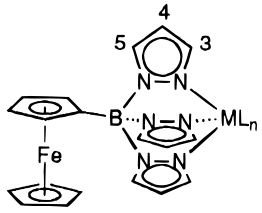

ML_n	**1-M**
Li	**1-Li**
Tl	**1-Tl**[a]
$ZrCl_3$	**1-Zr**
$Mo(CO)_3Li$	**1-MoLi**
$Mo(CO)_2(\eta^3$-methylallyl)	**1-Mo**

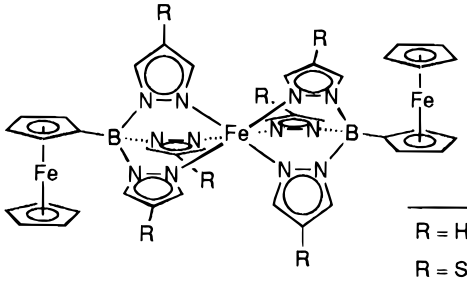

R = H	**1-Fe**[a]
R = $SiMe_3$	**1-FeSi**

Syntheses:

1-Li + $Mo(CO)_6$ —(i)→ **1-MoLi**

1-MoLi + $BrCH_2$-$C(CH_3)$=CH_2 —(ii)→ **1-Mo**

1-Li + $ZrCl_4$ —(iii)→ **1-Zr**

2 $Fc[B(4\text{-}SiMe_3pz)_3]H$ + $FeCl_2$ / 2 NEt_3 —(iv)→ **1-FeSi**

[a] See ref 10. Key: (i) CH_3CN, 5 h, reflux; (ii) CH_3CN, 12 h, reflux; (iii) CH_2Cl_2, −78 °C to rt; (iv) THF/toluene, rt.

Both compounds react with 3-bromo-2-methyl-1-propene in refluxing acetonitrile (12 h) to give the air-stable η^3-methylallyl complexes **1-Mo** and **2-Mo** in good yield.[16]

The homotrinuclear complex **1-Fe** is readily accessible by treating a slurry of $FeCl_2/NEt_3$ in THF with a toluene solution of the "free acid" **1-H** (2 equiv) at ambient temperature.[10] **1-Fe** suffers from low solubility in all common organic solvents, a problem which can easily be overcome by employing 4-(trimethylsilyl)pyrazole[17] rather than the unsubstituted parent compound. The silylated species **1-FeSi** (Scheme 1), which is prepared in the same way as **1-Fe**, is soluble even in hexane, provided a small amount of toluene is added.

The zirconium complex **1-Zr** can be obtained in high yield from a solid mixture of **1-Li** and 2 equiv of $ZrCl_4$, which is treated at −78 °C with CH_2Cl_2 and then slowly warmed to ambient temperature (Scheme 1).[18] Its trinuclear analogue **2-Zr**, however, is not formed under similar conditions. All attempts to synthesize **2-Zr** using either $ZrCl_4$ or $ZrCl_4$·2THF (4 equiv) and **2-Li** resulted in the decomposition of the discorpionate ligand. In all cases, ferrocenophane **D** (Figure 2) was identified as the main product by NMR spectroscopy. One Lewis basic pyrazolyl ring seems to be transferred from each of the boron

(11) Frasson, E.; Menegus, F.; Panattoni, C. *Nature* **1963**, *199*, 1087−1089.
(12) Berar, J. F.; Calvarin, G.; Pommier, C.; Weigel, D. *J. Appl. Crystallogr.* **1975**, *8*, 386−387.
(13) Jäkle, F.; Priermeier, T.; Wagner, M. *J. Chem. Soc., Chem. Commun.* **1995**, 1765−1766.
(14) Jäkle, F.; Priermeier, T.; Wagner, M. *Organometallics* **1996**, *15*, 2033−2040.
(15) Herdtweck, E.; Jäkle, F.; Opromolla, G.; Spiegler, M.; Wagner, M.; Zanello, P. *Organometallics* **1996**, *15*, 5524−5535.
(16) Trofimenko, S. *J. Am. Chem. Soc.* **1969**, *91*, 588−595.
(17) Birkofer, L.; Franz, M. *Chem. Ber.* **1972**, *105*, 1759−1767.
(18) Reger, D. L.; Tarquini, M. E. *Inorg. Chem.* **1982**, *21*, 840−842.

Scheme 2. Synthesis of Complexes **2-M** with Bifunctional Scorpionate Ligands[a]

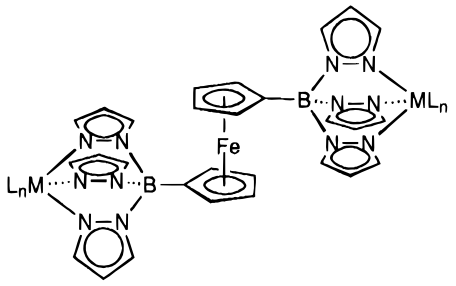

ML_n	**2-M**
Li	**2-Li**
Tl	**2-Tl**[a]
$Mo(CO)_3Li$	**2-MoLi**
$Mo(CO)_2(\eta^3$-methylallyl)	**2-Mo**
$ZrCl_3$	**2-Zr**

Syntheses:

2-Li + 2 $Mo(CO)_6$ —(i)→ **2-MoLi**

2-MoLi + 2 $BrCH_2$-$C(CH_3)$=CH_2 —(ii)→ **2-Mo**

2-Li + 2 $ZrCl_4$ —(iii)→ **2-Zr**

[a] See ref 10. Key: (i) CH_3CN, 5 h, reflux; (ii) CH_3CN, 12 h, reflux; (iii) CH_2Cl_2, −78 °C to rt.

Scheme 3. Decomposition of **2-Li** upon N-Methylation[a]

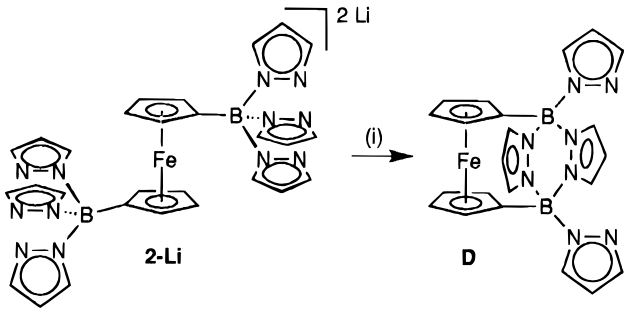

[a] See ref 14. Key: (i) $+2[Me_3O]BF_4$.

centers to the strongly Lewis acidic zirconium atoms. In contrast to **1-Li**, the remaining three-coordinate boron moieties can be stabilized in the case of the diborylated species by intramolecular donor-acceptor bonding and pyrazabole bridge formation, which is probably a driving force of the decomposition reaction. To further confirm this proposed mechanism, **2-Li** was treated with 2 equiv of the Meerwein salt $[Me_3O]BF_4$ in order to methylate one pyrazolyl ring of each scorpionate unit and thus to transform it into a better leaving group. The reaction led to a mixture of compounds, but the main product again was the ferrocenophane **D** (Scheme 3).

We may thus conclude, that those transition metal compounds are best suited for the formation of discorpionate complexes **2-M**, which possess low Lewis acidity together with three weakly bound ligands, that can easily be replaced by the tris-(1-pyrazolyl)borate unit as a whole.

Spectroscopic Properties of $FcB(pz)_3ML_n$ and 1,1′-$fc[B(pz)_3ML_n]_2$. The main initially apparent feature in the NMR spectra of most complexes **1-M** and **2-M** is an extreme broadening of the pyrazolyl resonances at ambient temperature due to some fluxionality in these molecules, which is moderate on the NMR time scale. Only the Li and Tl derivatives show

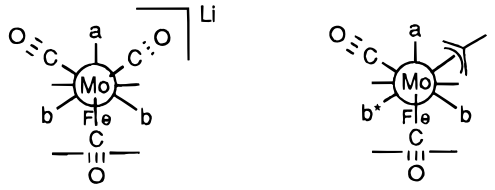

Figure 3. Schematic representation of achiral **1-MoLi** and one chiral conformation of **1-Mo**.

sharp, well-resolved ^{1}H- and ^{13}C-NMR signals under these conditions. NMR spectroscopical investigations in the temperature range between −90 °C and ambient temperature revealed further differences between complexes of high local symmetry at ML_n (**1-Zr**, **1-MoLi**, **2-MoLi**) and compound **1-Mo**, where substitution of an η^3-methylallyl group for one CO ligand leads to a lower symmetry at the ML_n fragment. At low temperature **1-Zr** and **1-MoLi** show two sets of signals in the pyrazolyl region of the ^{1}H- and ^{13}C-NMR spectra (integral ratio 2:1), while **1-Mo**, and **2-Mo** exhibit three sets of resonances (integral ratio 1:1:1). This indicates the presence of two magnetically equivalent pyrazole rings in the former molecules, whereas different chemical environments for all three pyrazole units have to be assumed in the latter. It may thus be concluded that there are two different sites of hindered molecular motion in **1-M**, one being the rotation of the ferrocenyl substituent around the boron−carbon bond and the other the rotation of the ML_n fragment relative to the scorpionate ligand. At low temperature, the ferrocenyl substituent is likely to be located in one of the three uncongested clefts between two pyrazole rings in order to minimize nonbonding interactions. This leaves the third pyrazolyl substituent in the unique position orthogonal to the cyclopentadienyl rings (Scheme 1). Our interpretation is further substantiated by the fact that the resonance of the proton in position 5 of the unique pyrazolyl ring experiences an unusually high shielding (e.g. **1-Zr**: $\delta(^1H) = 6.73$), which can be attributed to the magnetic anisotropy effect of the cyclopentadienyl ring.

The expected hindered rotation of the ML_n fragment has no visible effect on the NMR spectra of **1-Zr** and **1-MoLi**. In the case of **1-Mo**, however, the three magnetically nonequivalent pyrazolyl rings demonstrate a further symmetry reduction in the molecule, which leads to the conclusion that the η^3-methylallyl substituent must be located in a different segment of the scorpionate ligand than the ferrocenyl substituent. Consequently, four rather than two resonances for the substituted C_5H_4 ring are visible at −70 °C in the ^{1}H NMR spectrum of the latter. We can thus summarize that **1-Mo** preferentially adopts a chiral conformation at low temperatures in solution (Figures 3 and 4), as has been found also in the solid state by a crystal structure determination of this molecule (see below).

From the coalescence temperatures T_c of the proton signals, activation barriers $\Delta G^{\ddagger}$ of the hindered rotation in the monoscorpionate complexes have been determined: **1-MoLi**, 60 ± 2 kJmol^{-1}, CD_3CN; **1-Mo**, 56 ± 2 kJmol^{-1}, [D_8]toluene; **1-Zr**, 54 ± 2 kJmol^{-1}, CD_2Cl_2 ($\Delta G^{\ddagger} = 19.14T_c(10.32 + \log(T_c\, k_c^{-1})$; $k_c = 2.22\ \Delta\nu$).[19] In the case of **1-MoLi** and **1-Zr**, $\Delta G^{\ddagger}$ is the energy barrier of the hindered ferrocenyl rotation, whereas in **1-Mo** no assignment of $\Delta G^{\ddagger}$ to either hindered ferrocenyl or $Mo(CO)_2(\eta^3$-methylallyl) rotation can be made.

(19) Friebolin, H. *Basic One and Two Dimensional NMR Spectroscopy*; Verlag Chemie: Weinheim, Basel, Cambridge, New York, 1992.

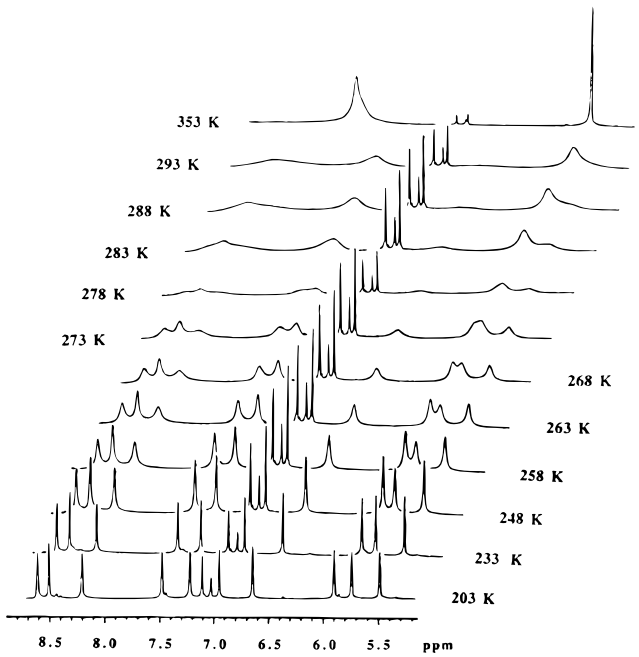

Figure 4. Variable-temperature ^{1}H FT NMR spectra of **1-Mo** in [D_8]toluene (pyrazolyl region given).

Table 1. Summary of Crystallographic Data for $FcB(pz)_3Mo(CO)_2[\eta^3\text{-}H_2CC(CH_3)CH_2]$ **(1-Mo)**

chem formula	$C_{25}H_{25}BFeMoN_6O_2$	fw	604.11
a	8.756(1) Å	space group	*P*$\bar{1}$ (No. 2)
b	12.154(1) Å	*T*	−50 ± 1 °C
c	12.927(1) Å	λ	0.710 73 Å
α	105.26(1)°	ρ_{calcd}	1.642 g·cm^{-3}
β	102.29(1)°	μ	11.4 cm^{-1}
γ	105.09(1)°	R_1[a]	0.031
V	1221.6(2) Å^3	wR_2[b]	0.088
Z	2		

[a] R_1: $\Sigma(||F_o| - |F_c||)/\Sigma|F_o|$. [b] w$R_2$: $[\Sigma w(F_o^2 - F_c^2)^2/\Sigma w(F_o^2)^2]^{1/2}$.

The results of a dynamic NMR study of the trinuclear complex **2-Mo** are in full consonance with the previous findings. At ambient temperature, the ^{1}H- and ^{13}C-NMR spectra show very broad resonances and a signal pattern, which makes their assignment rather difficult. This situation changes completely when spectra are recorded at +80 and −70 °C, respectively. For the pyrazolyl rings, a single set of signals is found at elevated temperatures, whereas three sets of resonances (integral ratio 1:1:1) are observed at −70 °C. Most interestingly, the protons of the ferrocenyl core give rise to eight signals of equal intensity at low temperature, which points toward a *rac*/*meso* mixture of diastereomers in the sample. Since both prochiral units are equally close to the ferrocene backbone, but rather far apart from each other, the pyrazolyl rings possess the same NMR shifts both in the *rac* and in the *meso* isomer, while different chemical shifts for *rac*- and *meso*-**2-Mo** are found in the ferrocenyl region.

Line broadening due to hindered molecular motion is also apparent in **1-FeSi**. However, well-resolved spectra recorded at +80 °C ([D_8]toluene) indicate the central iron atom in this compound to be in the low-spin state, thereby testifying to the strong ligand field exerted by $FcB(4\text{-}SiMe_3pz)_3^-$.[20]

Molecular Structure of 1-Mo. The molybdenum(II) complex **1-Mo** crystallizes from acetonitrile in the triclinic space group *P*$\bar{1}$ (Table 1).

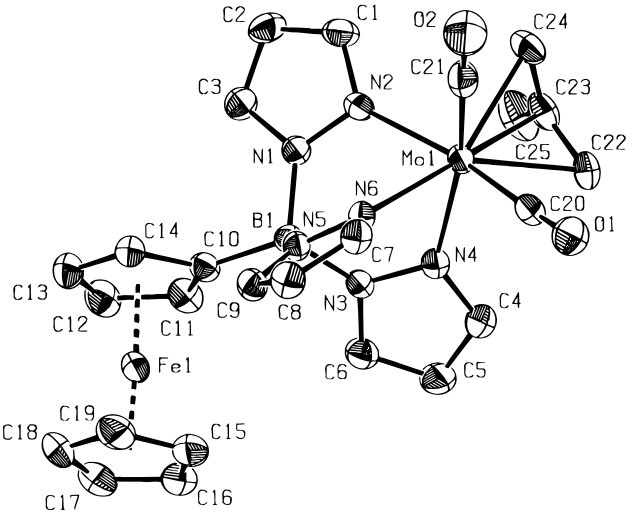

Figure 5. PLATON plot of **1-Mo**. Thermal ellipsoids are drawn at the 50% probability level.

Table 2. Selected Bond Distances (Å) and Angles (deg) and Angles between Planes (deg) of Compound **1-Mo**

B(1)−C(10)	1.602(4)	Mo(1)−N(2)	2.242(3)
B(1)−N(1)	1.559(4)	Mo(1)−N(4)	2.280(3)
B(1)−N(3)	1.548(3)	Mo(1)−N(6)	2.204(3)
B(1)−N(5)	1.564(4)	Mo(1)−C(22)	2.333(4)
N(1)−N(2)	1.364(4)	Mo(1)−C(23)	2.246(3)
N(3)−N(4)	1.375(4)	Mo(1)−C(24)	2.345(4)
N(5)−N(6)	1.366(4)		

N(1)−B(1)−N(3)	110.0(2)	N(2)−Mo(1)−N(4)	83.2(1)
N(1)−B(1)−N(5)	106.9(2)	N(2)−Mo(1)−N(6)	79.5(1)
N(3)−B(1)−N(5)	105.0(2)	N(4)−Mo(1)−N(6)	77.5(1)
C(10)−B(1)−N(1)	106.6(2)	C(20)−Mo(1)−C(21)	80.5(1)
C(10)−B(1)−N(3)	114.8(2)	C(22)−C(23)−C(24)	112.8(3)
C(10)−B(1)−N(5)	113.2(2)		

N(1)−C(3)// N(3)−C(6)	39.2(2)	N(1)−C(3)// C(10)−C(14)	77.2(2)
N(1)−C(3)// N(5)−C(9)	61.4(2)	C(10)−C(14)// C(15)−C(19)	3.3(2)
N(3)−C(6)// N(5)−C(9)	79.4(2)	O(1)C(20)C(21)O(2)// C(22)C(23)C(24)C(25)	9.4(3)

The most obvious difference in the solid-state structures of **1-Mo** and the thallium(I) derivative **1-Tl**[10] is the fact that the tris(1-pyrazolyl)borate moiety acts as a true tridentate ligand to the molybdenum center (Figure 5).

In **1-Tl**, however, each thallium atom binds to two pyrazole rings of one scorpionate ligand and to one pyrazole ring of another ligand, thereby generating a polymeric structure.[10] Its Tl−N bond lengths are considerably longer than those found in the other structurally characterized tris(1-pyrazolyl)borate complexes of Tl(I), which are all featuring discrete molecules with tridentate $B(pz)_3$ units. In contrast, the Mo−N bond lengths in **1-Mo** do not show any particularities compared to the crystal structures of other (η^3-allyl)dicarbonyl[tris(1-pyrazolyl)borato]molybdenum complexes (Table 2).[21]

As usual, the shortest Mo−N bond is observed for the pyrazole ring located in *trans* position to the η^3-allyl substituent (Mo(1)−N(6) = 2.204(3) Å). Two longer Mo−N bonds are found *trans* to the carbonyl ligands (Mo(1)−N(2) = 2.242(3) Å; Mo(1)−N(4) = 2.280(3) Å). When the allyl ligand is considered as a single substituent, the complex possesses a six-coordinate octahedral geometry. The allyl substituent adopts

(20) Sohrin, Y.; Kokusen, H.; Matsui, M. *Inorg. Chem.* **1995**, *34*, 3928−3934.

(21) Ward, Y. D.; Villanueva, L. A.; Allred, G. D.; Payne, S. C.; Semones, M. A.; Liebeskind, L. S. *Organometallics* **1995**, *14*, 4132−4156.

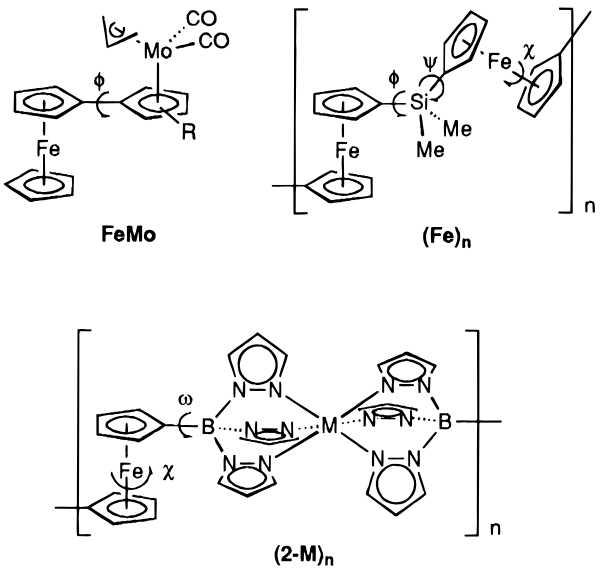

Figure 6. Heterobimetallic cyclopentadienyl complex **FeMo**, closely related to the scorpionate complex **1-Mo**, poly(ferrocenylenesilane) **(Fe)*n***, and coordination polymer **(2-M)*n***.

an *exo* conformation with respect to the $Mo(CO)_2$ fragment, and the plane defined by the four allyl carbon atoms is nearly periplanar to that spanned by the two carbonyl substituents (angle between both planes: 9.4(3)°). The ferrocenyl substituent is rotated into one of the three uncongested clefts made up by the three pyrazole moieties of the scorpionate ligand. This places one pyrazole unit (N(1) to C(3)) in a position almost perpendicular to the cyclopentadienyl rings (Table 2) and thus minimizes nonbonding interactions between the hydrogen atoms of the pyrazole rings and the central iron atom of the ferrocene fragment (a similar conformation is observed in **1-Tl**). However, the situation around the boron center still seems to be somewhat crowded leading to a slight dislocation of the boron atom out of the plane defined by the attached cyclopentadienyl ring ($\alpha^* = COG-C(10)-B(1) = 10.3°$; COG = center of gravity of the cyclopentadienyl ring). The ferrocenyl unit and the allyl substituent occupy two different clefts of the tris(1-pyrazolyl)borate moiety, which results in a chiral conformation of the molecule, as has already been proposed from the low-temperature NMR spectra.

Metal−metal distances are of crucial importance for all oligometallic complexes. **1-Mo** exhibits an Fe−Mo separation of 6.75 Å in the solid state, which is probably not very much different in solution given the pronounced structural rigidity of the molecular framework. A comparison of **1-Mo** with the analogous η^5-C_5R_4 complex **FeMo**[22] (C_5R_4 = indenyl; Figure 6) reveals the latter to adopt a *trans* conformation of the $(C_5H_5)Fe$ and $Mo(CO)_2(\eta^3$-$C_3H_5)$ fragments in the solid state, leading to an Fe−Mo distance of 5.37 Å. From the crystal structure data a value *d*[Fe−Mo] of approximately 3.99 Å can be deduced for the *cis* conformation. If we assume an unhindered rotation around the C−C single bond connecting both mononuclear building blocks, the average Fe−Mo separation of **FeMo** in solution is intermediate between both extremes.

One major topic of our research is the synthesis of coordination polymers **(2-M)*n***, which incorporate transition metals in the backbone and consist of ions M^{n+} (M = Cr, Mn, Fe, Co) connected by the bifunctional linker **2**. Both the electronic and the magnetic properties of these polymers can be expected to depend on the Fe−M distances. The value of 6.75 Å observed for **1-Mo** may serve as an initial guess for Fe−M separations in **(2-M)*n***. In comparison, the Fe−Fe distances in Fc[−$SiMe_2$fc−]$_4$H, an oligomeric model for poly(ferrocenylenesilane) **(Fe)*n***,[23] which is one of the most prominent organometallic polymers (Figure 6), were found to possess similar values of 6.06 and 6.91 Å in the solid state.[24] However, there is an important difference between **(Fe)*n*** and **(2-M)*n***: The Fe−Fe distances in poly(ferrocenylenesilane) change with the relative disposition of any two neighboring ferrocenes as described by the torsion angles ϕ and ψ. A molecular mechanics study on dimeric Fc[−$SiMe_2$fc−]H using the ESFF forcefield[25] gave a global energy minimum with an iron separation of 5.95 Å.[23] Two less stable minima do also exist, corresponding to Fe−Fe distances of 5.61 and 7.08 Å. When both iron atoms are oxidized, electrostatic repulsion in the dication $\{Fc[-SiMe_2fc-]H\}^{2+}$ leads to a global minimum with an increased iron separation of 7.19 Å. Conformational flexibility of the polymer chain **(2-M)*n*** arises, as in the case of **(Fe)*n***, from mutual rotation of the cyclopentadienyl rings in the ferrocene cores (torsion angle χ; Figure 6). A second perpendicular axis of rotation in **(2-M)*n*** is defined by the two boron atoms of adjacent scorpionate ligands (torsion angle ω; Figure 6). It is important to note, that in contrast to **(Fe)*n***, the Fe−M distances in **(2-M)*n*** are well-defined, because they do not change upon rotation around χ or ω.

Electrochemical Properties of $FcB(pz)_3ML_n$ and 1,1′-$fc[B(pz)_3ML_n]_2$. Analysis[26] of the cyclic voltammograms of **1-Tl** with scan rates varying from 0.02 to 1.00 V s^{-1} shows the following: (a) The i_{pc}/i_{pa} ratio progressively increases from 0.7 at 0.02 V s^{-1} to 1.0 at 1.00 V s^{-1}. (b) The current function $i_{pa}/v^{1/2}$ remains constant. (c) The peak-to-peak separation progressively increases from 76 mV at 0.02 V s^{-1} to 110 mV at 1.00 V s^{-1}. Since the one-electron oxidation of ferrocene displays a quite similar trend in peak-to-peak separation, these parameters are diagnostic for an electrochemically reversible one-electron oxidation coupled to chemical complications. Controlled potential coulometry at $E_w = +0.6$ V shows the consumption of one electron per molecule. Upon exhaustive oxidation the original yellow solution turns pale green, and voltammetric tests indicate that about 50% of the instantaneously electrogenerated monocation $[\mathbf{1\text{-}Tl}]^+$ have decomposed at this stage. Confirming that the introduction of the thallium(I)−scorpionate fragment into the ferrocene core facilitates degradation of the oxidized species, **2-Tl** displays an irreversible one-electron oxidation process.

At variance with **1-Tl**, **1-Zr** exhibits a chemically reversible, ferrocene-centered one-electron oxidation ($[\mathbf{1\text{-}Zr}]^+$: $\lambda_{max} = 650$ nm). The fact that the redox potentials for **1-Tl** and **1-Zr** (+0.38 and +0.41 V, respectively) are very close to that of unsubstituted ferrocene (+0.39 V) testifies to the low electronic perturbation caused by the present tris(1-pyrazolyl)borate fragments.

The cyclic voltammetric profiles of **1-Mo** and **2-Mo** are compared in Figure 7. As shown in Figure 7a, **1-Mo** is characterized by two subsequent anodic processes with features of chemical reversibility.

Controlled potential coulometry in correspondence to the most anodic process ($E_w = +0.8$ V) consumes two electrons per

(22) Begley, M. J.; Mountford, P.; Stewart, P. J.; Swallow, D.; Wan, S. *J. Chem. Soc., Dalton Trans.* **1996**, 1323−1332.

(23) Barlow, S.; Rohl, A. L.; Shi, S.; Freeman, C. M.; O'Hare, D. *J. Am. Chem. Soc.* **1996**, *118*, 7578−7592.

(24) Rulkens, R.; Lough, A. J.; Manners, I. *J. Am. Chem. Soc.* **1994**, *116*, 797−798.

(25) Shi, S.; Yan, L.; Shaulsky, J.; Thatcher, T. A New Forcefield, ESFF, for Molecular Modelling of Organic, Inorganic and Organometallic Systems. Manuscript in preparation.

(26) Brown, E. R.; Sandifer, J. In *Physical Methods in Chemistry. Electrochemical Methods*; Rossiter, B. W., Hamilton, J. F., Eds.; Wiley: New York, 1986.

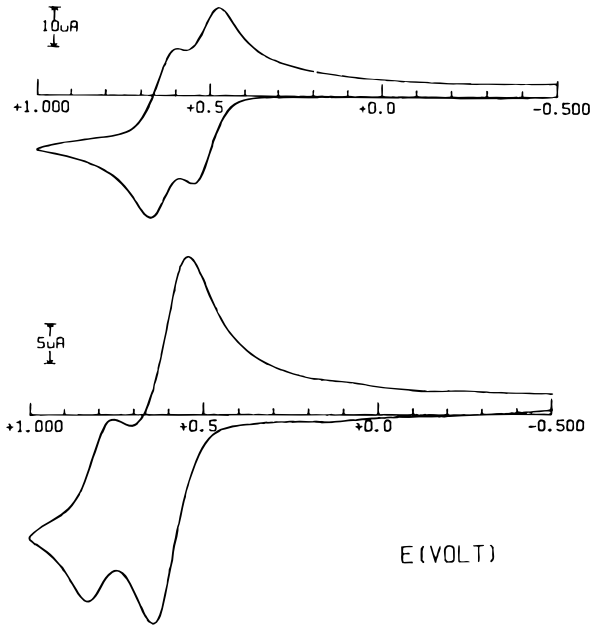

Figure 7. Cyclic voltammograms recorded at a platinum electrode on a CH_2Cl_2 solution containing $[NBu_4][PF_6]$ (0.2 mol dm^{-3}) and (a) **1-Mo** (1.3×10^{-3} mol dm^{-3}) and (b) **2-Mo** (0.9×10^{-3} mol dm^{-3}). Scan rate: 0.2 V s^{-1}.

molecule, thus indicating that two distinct one-electron steps are involved in the oxidation of **1-Mo**. Step-by-step controlled potential electrolysis shows the following: (a) The first oxidation process is chemically reversible; the solution of **[1-Mo]**$^+$ resulting from exhaustive electrolysis ($E_w = +0.55$ V) assumes a deep green color ($\lambda_{max} = 635$ nm) and displays stretching CO frequencies substantially unaltered with respect to the original ones. (b) The second oxidation process ($E_w = +0.8$ V) causes slow decomposition of the oxidation product, thus suggesting the dication **[1-Mo]**$^{2+}$ to be only a transient species. The first one-electron removal is most likely centered on the ferrocene fragment, whereas the second one-electron removal is centered on the molybdenum(II) appendix.

In contrast, Figure 7b shows the single-stepped two-electron oxidation of the two Mo(II) fragments in **2-Mo** to precede the one-electron oxidation of the ferrocene group. This datum is confirmed by the fact that exhaustive two-electron oxidation at $E_w = +0.65$ V affords a brown-green solution, which in the region between 600 and 700 nm of the UV/vis spectrum does not exhibit any absorption typical of ferrocenium species. Moreover, in the IR spectrum the two ν(CO) bands undergo a shift of about 10 cm^{-1} toward higher frequencies. The solution resulting from the overall three-electron oxidation ($E_w = 0.9$ V) is highly unstable and tends to restore the dication oxidation state.

It is interesting to compare the electronic environments of the metal centers in **1-Mo** and **FeMo**, which are formally related by the scorpionate−cyclopentadienide analogy. The CO stretching frequencies, which are a first spectroscopic register of the charge density at molybdenum, show essentially the same values in both components (**1-Mo**, ν(CO) = 1847, 1941 cm^{-1}; **FeMo** ($C_5R_4 = C_5H_2Me_2$), ν(CO) = 1851, 1936 cm^{-1}). Strikingly similar values are also observed for the redox potentials of the Mo(II)/Mo(III) couples (**1-Mo**, +0.63 V; **FeMo** ($C_5R_4 = C_5H_2Me_2$), +0.57 V; referenced to Fc-H/Fc-H$^+$, +0.39 V). It may therefore be concluded that the substitution of the scorpionate claw for the cyclopentadienide ligand has almost no consequence on the charge density at the Mo center. A more pronounced effect, however, is evident for the Fc core. The pending scorpionate complex seems to relieve more charge density than the cyclopentadienyl appendix, as indicated by a more anodic Fe(II)/Fe(III) oxidation potential in the former compound (**1-Mo**, +0.51 V; **FeMo** ($C_5R_4 = C_5H_2Me_2$), +0.39 V; referenced to Fc-H/Fc-H$^+$, +0.39 V). This is in accord with the finding that Mo(II)/Mo(III) oxidation precedes that of the Fe(II) center in **2-Mo**, which may be attributed to the presence of two electron-withdrawing molybdenum scorpionates attached to the fc core. Thus, an influence of the molybdenum unit on the central iron atom is apparent in **1-Mo** and **2-Mo**. On the other hand, the appearance of a single Mo(II)Mo(II)/Mo(III)Mo(III) oxidation wave indicates that the 1,1′-bis[tris(1-pyrazolyl)borate] assembly of **2-Mo** does not permit electronic communication between the two molybdenum subunits.

Finally a cyclic voltammogram of **1-FeSi** displays a first oxidation followed by a second oxidation twice as high as the first one. Both processes show features of chemical reversibility. The first exhaustive one-electron oxidation ($E_w = +0.2$ V) of **1-FeSi** causes the originally pale red solution to turn ruby red, giving rise to a broad band encompassing the region from 350 to 600 nm in the UV/vis spectrum. Further exhaustive two-electron oxidation ($E_w = +0.7$ V) results in a brown solution, and a shoulder at $\lambda = 630$ nm adds to the above reported visible spectrum. It is thus immediately apparent that the one-electron oxidation of the unique Fe(II) atom precedes the single-stepped two-electron oxidation of the two lateral ferrocenyl fragments. The chemical reversibility of both redox changes is testified by the fact that the cyclic voltammetric profiles recorded on the solutions resulting from the two exhaustive oxidation steps are quite complementary to that of **1-FeSi** *before* exhaustive oxidation. It is evident that the two peripheral Fc fragments are electronically independent from each other but seem to suffer from electrostatic interactions with the central Fe(III) ion in **[1-FeSi]**$^+$, as suggested by the rather high redox potential of the Fc units ($E^{\circ\prime} = +0.57$ V). A comparison with the electrochemical behavior of the system $Fc[-CMe_2fc-]_2H$, which is closely related to **(Fe)$_n$** (Figure 6), is particularly revealing. The cyclic voltammogram of this molecule displays three resolved oxidation waves with separations between successive waves of 14 and 20 mV.[27] These data have been interpreted in the following way: The first oxidation occurs at the central iron atom, leading to a species Fe(II)−Fe(III)−Fe(II). The dication resulting from the second oxidation minimizes repulsive electrostatic interactions by forming a species Fe(III)−Fe(II)−Fe(III) rather than Fe(III)−Fe(III)−Fe(II).[27] For this charge redistribution to occur, similar oxidation potentials of the three Fe(II) centers are required, which is certainly true for $Fc[-CMe_2fc-]_2H$. In **1-FeSi**, however, there is a pronounced difference in the redox potentials of the central iron atom ($E^{\circ\prime} = +0.06$ V) and the Fc units, even if we take into account that the $E^{\circ\prime}$ value of 0.57 V found for the oxidation of the two Fc substituents is more anodic than the real unperturbed potential, since it reflects the coulombic repulsion within the molecule. It is thus important to note that the lack of communication between the ferrocenyl end groups in **1-FeSi** has not necessarily to be attributed to the specific architecture of the molecular backbone but may well be a result of the bad match between the redox potentials of the different iron centers. In the ferrocene-capped cobalt clathrochelate $Co(nox)_3[B(C_5H_4)Fe(C_5H_5)]_2$ (nox: 1,2-cyclohexanedione dioximate(2−)), for example, which is another system related to **1-FeSi** featuring electronically communicating metal sites, the difference in the redox potentials of the Co(II)/Co(III) couple and the Fe(II)/

(27) Barlow, S.; Murphy, V. J.; Evans, J. S. O.; O'Hare, D. *Organometallics* **1995**, *14*, 3461−3474.

Table 3. Formal Electrode Potentials and Peak-to-Peak Separations for the Oxidation Processes Exhibited by the Present Ferrocene-Based Metal−Scorpionates[a]

	ferrocene-centered process		metal-centered process	
complex	$E^{\circ\prime}$	ΔE_p[b]	$E^{\circ\prime}$	ΔE_p[b]
1-Tl	+0.38[c]	84		
2-Tl	+0.37[d]			
1-Zr	+0.41	81		
1-Mo	+0.51	69	+0.63	62
2-Mo	+0.80	70	+0.60[e]	90
1-FeSi	+0.57[e]	76	+0.06	74
$Fe(C_5H_5)_2$	+0.39	89		

[a] Formal electrode potentials in V, vs SCE, and peak-to-peak separations in mV, in CH_2Cl_2 solution containing $[NBu_4][PF_6]$ (0.2 mol dm^{-3}) as supporting electrolyte. [b] Measured at 0.2 V s^{-1}. [c] Complicated by slow chemical reactions. [d] Peak potential value for irreversible processes. [e] Two-electron process.

Fe(III) couple is only 0.16 V.[28] In this context, the $SiMe_3$ groups of **1-FeSi** may certainly not be regarded as innocent spectators as far as the electron density of the ligand is concerned. For comparison, the Fe(II)/Fe(III) couple in the nonsilylated parent complex $Fe[HB(pz)_3]_2$ occurs at +0.28 V[29] (referenced to $E^{\circ\prime}(FcH/FcH^+) = 0.39$ V), which is 0.22 V more anodic than in the case of **1-FeSi**.

Table 3 summarizes the formal electrode potentials for the above discussed electron transfers. In contrast to **1-Tl**, **2-Tl**, and **1-Zr**, the tris(1-pyrazolyl)borate complexes of **1-Mo**, **2-Mo**, and **1-FeSi** relieve significant electron density from the linked ferrocenyl group(s). Except for **1-Tl** and **2-Tl**, the substantial electrochemical reversibility of all the redox changes indicates that no significant structural reorganizations accompany the different electron removal steps.[30]

Conclusion

Ferrocene-based mono- and bifunctional tris(1-pyrazolyl)-borate ligands provide a facile route to heterobimetallic and -trimetallic assemblies incorporating transition metal complex fragments as different in nature as Tl^I, $Mo^0(CO)_3Li$, $Mo^{II}(CO)_2(\eta^3$-methylallyl), Fe^{II}, and $Zr^{IV}Cl_3$. High-yield syntheses are available for most of these compounds. However, complications may occur when the bifunctional ligand 1,1′-$fc[B(pz)_3]_2^{2-}$, **2**, is treated with strong Lewis acids like $ZrCl_4$ or the CH_3^+ ion. These electrophiles tend to interact (initially) with one pyrazolyl ring only, rather than with the tridentate claw as a whole. In these cases, pyrazolyl abstraction and stabilization of the remaining three-coordinate boron species by intramolecular donor−acceptor pairing leads to the formation of ferrocenophane **D** with pyrazabole bridge.

The ferrocenyltris(1-pyrazolyl)borate ligand is able to establish different binding modes. Two of them have so far been characterized by X-ray crystallography: **1-Tl** adopts a unique polymeric structure in the solid state, while **1-Mo** features discrete molecules with the scorpionate moiety acting as a tridentate ligand in the usual way. In contrast to the prominent class of fulvalene- (and related) bridged heterooligometallic compounds, the Fe−M distances in polynuclear complexes **1-M** and **2-M** are well-defined and not subject to changes upon intramolecular motion. Comparatively high barriers of ferrocenyl rotation around the C-B bonds are observed for all compounds in solution, except for **1-Li** and **1-Tl**. In the case of **1-Mo** and **2-Mo**, chiral molecular geometries are thus evident at low temperatures.

Apart from the thallium(I) complexes, where ferrocene oxidation is coupled to chemical complications, all other compounds under investigation give good electrochemical responses. Ferrocene oxidation is generally reversible, as is the oxidation of the molybdenum centers in **2-Mo** and of the central iron atom in **1-FeSi**.

The comparison of the scorpionate derivative **1-Mo** with the cyclopentadienide analog **FeMo** reveals essentially the same charge density at the molybdenum atoms, thus testifying to the close relationship of both ligand systems in this case. The order of the Fe(II)/Fe(III) and Mo(II)/Mo(III) redox potentials becomes inverted upon switching from **1-Mo** to **2-Mo** due to the electron-withdrawing effect of two molybdenum scorpionate substituents in the latter case. Consequently, the Fe(II)/Fe(III) redox couple possesses a remarkably anodic potential ($E^{\circ\prime}$ = 0.80 V). In **2-Mo**, no direct influence of the two pending molybdenum centers on each other could be detected.

The Fc substituents in **1-FeSi** do not show any indication of electronic communication, as well. One reason probably lies in the pronounced difference of the redox potentials of the central iron atom and the ferrocenyl units. However, there is evidence for electrostatic interactions between the central iron atom and the Fc end groups in the mixed-valence states of **1-FeSi**. These assumptions are currently subject to further investigations.

The bifunctional linker **2** offers an opportunity to create novel organometallic polymers **(2-M)$_n$** containing various transition metals in the polymer backbone. Since scorpionates resemble the cyclopentadienide ligand in many respects, compounds **(2-M)$_n$** may be considered as readily available analogs of polyferrocenylenes and poly(ferrocenylenesilanes). Highly soluble oligometallics can be obtained by employing silylated scorpionate ligands, as demonstrated by the trinuclear oligomer **1-FeSi**, which is even soluble in hexane/toluene mixtures (10:1).

Experimental Section

General Considerations. All reactions and manipulations of air-sensitive compounds were carried out in dry, oxygen-free argon using standard Schlenkware or in an argon-filled drybox. Solvents were freshly distilled under N_2 from Na/K alloy−benzophenone (toluene, hexane, Et_2O, *n*-Bu_2O) or from CaH_2 (CH_2Cl_2, CH_3CN) prior to use. IR: solvent CH_3CN or CH_2Cl_2 (organic and organometallic compounds), Perkin-Elmer 1650 FTIR. NMR: Jeol JMN-GX 400 and Bruker DPX 400 (abbreviations: s = singlet, d = doublet, tr = triplet, vtr = virtual triplet, br = broad, pz = 1-pyrazolyl). NMR spectra were recorded at ambient temperature, unless stated otherwise. The letters a and b in the assignment of NMR spectra indicate magnetically nonequivalent pyrazole rings. ^{11}B and ^7Li NMR shifts are given relative to external $BF_3{\cdot}Et_2O$ and aqueous LiCl, respectively. MS (CI, FAB mode): Finnigan MAT 90. Elemental analyses: Microanalytical laboratory of the Technische Universität München.

The compounds $FcBBr_2$,[6] 1,1′-$fc(BBr_2)_2$,[7] and 4-(trimethylsilyl)-pyrazole[17] were synthesized according to literature procedures.

Synthesis of 1-Li. Neat $HNMe_2$ (1.58 g, 35.10 mmol) was added at −78 °C to a solution of $FcBBr_2$ (3.01 g, 8.49 mmol) in 80 mL of toluene with efficient stirring. The mixture was allowed to warm to ambient temperature, kept at 70 °C for 2 h (dry ice condenser), and filtered to remove the precipitated $[H_2NMe_2]Br$. The resulting solution of $FcB(NMe_2)_2$ was added without further purification at ambient temperature to a THF solution of freshly prepared Li(pz) (0.63 g, 8.51 mmol) and Hpz (1.15 g, 16.90 mmol). The mixture was refluxed for 12 h and the solvent removed under reduced pressure. The yellow microcrystalline solid obtained was treated two times with 20 mL of toluene and dried in vacuo. Yield: 3.26 g (95%).

(28) Murguia, M. A.; Borchardt, D.; Wherland, S. *Inorg. Chem.* **1990**, *29*, 1982−1986.
(29) Armstrong, W. H.; Spool, A.; Papaefthymiou, G. C.; Frankel, R. B.; Lippard, S. J. *J. Am. Chem. Soc.* **1984**, *106*, 3653−3667.
(30) Togni, A.; Hobi, M.; Rihs, G.; Rist, G.; Albinati, A.; Zanello, P.; Zech, D.; Keller, H. *Organometallics* **1994**, *13*, 1224−1234.

^{11}B NMR (128.3 MHz, CD_3CN): δ −0.5 ($h_{1/2}$ = 150 Hz). ^{1}H NMR (400 MHz, CD_3CN): δ 4.20 (s, 5H, C_5H_5), 4.25, 4.50 (2 × vtr, 2 × 2H, J(H,H) = 1.5 Hz, C_5H_4), 6.08 (vtr, 3H, J(H,H) = 2.0 Hz, pz-H4), 7.51, 7.93 (2 × d, 2 × 3H, J(HH) = 2.0 Hz, pz-H3,5). ^{13}C NMR (100.5 MHz, CD_3CN): δ 69.8 (C_5H_5), 70.9, 75.8 (C_5H_4), n.o. (C_5H_4-*ipso*), 103.9 (pz-C4), 135.3, 139.9 (pz-C3,5). FAB-MS: *m/z* 397 [(M^- − Li); 50%]. Anal. Calcd for $C_{19}H_{18}BFeLiN_6$ (403.87): C, 56.51; H, 4.46; Li, 1.7; N, 20.80. Found: C, 56.43; H, 4.59; Li, 1.6; N, 20.81.

Synthesis of 1-Zr. Cold CH_2Cl_2 (20 mL; −78 °C) was added to a solid mixture of **1-Li** (0.45 g, 1.11 mmol) and $ZrCl_4$ (0.52 g, 2.23 mmol), the resulting suspension was slowly warmed to ambient temperature and stirred for 12 h. A clear solution was observed at 0 °C, and a white precipitate formed at higher temperatures. Insoluble material was collected on a frit (G4) and extracted two times with 10 mL of CH_2Cl_2. The solvent was removed from the filtrates in vacuo, and a yellow solid residue was obtained, which gave orange needles of **1-Zr** after recrystallization from toluene/CH_2Cl_2. Yield: 0.53 g (80%).

^{11}B NMR (128.3 MHz, CD_2Cl_2): δ 1.7 ($h_{1/2}$ = 100 Hz). ^{1}H NMR (400.0 MHz, CD_2Cl_2): δ 4.30 (s, 5H, C_5H_5), 4.36, 4.67 (2 × vtr, 2 × 2H, J(HH) = 1.8 Hz, C_5H_4), 6.33 (br, 3H, pz-H4), 8.18 (d, 3H, J(HH) = 1.8 Hz, pz-H3), 8.3 (very br, 3H, pz-H5). ^{1}H NMR (400.0 MHz, CD_2Cl_2, −90 °C): δ 4.25 (s, 5H, C_5H_5), 4.27, 4.59 (2 × vtr, 2 × 2H, J(HH) = 1.8 Hz, C_5H_4), 6.10 (vtr, 1H, J(HH) = 1.8 Hz, pz-H4a), 6.40 (vtr, 2H, J(HH) = 1.8 Hz, pz-H4b), 6.71 (d, 1H, J(HH) = 1.8 Hz, pz-H5a), 8.06 (d, 1H, J(HH) = 1.8 Hz, pz-H3a), 8.13 (d, 2H, J(HH) = 1.8 Hz, pz-H3b), 8.72 (d, 2H, J(HH) = 1.8 Hz, pz-H5b). ^{13}C NMR (100.5 MHz, CD_2Cl_2): δ 69.5 (C_5H_5), 71.9, 74.8 (C_5H_4), n.o. (C_5H_4-*ipso*), 105.5 (pz-C4), 137.1, 145.0 (pz-C3,5). ^{13}C NMR (100.5 MHz, CD_2Cl_2, −90 °C): δ 68.6 (C_5H_5), 71.0, 73.6 (C_5H_4), n.o. (C_5H_4-*ipso*), 104.5 (pz-C4a), 105.1 (pz-C4b), 135.8 (pz-C3,5b), 137.6, 143.7 (pz-C3,5a), 143.8 (pz-C3,5b). CI-MS: *m/z* 592 [(M^-); 100%], 407 [(M^- − (C_5H_4)Fe(C_5H_5)); 5%]. Anal. Calcd for $C_{19}H_{18}BCl_3FeN_6Zr$ (594.50): C, 38.38; H, 3.03; Cl, 17.89; N, 14.14. Found: C, 37.98; H, 3.02; Cl, 17.76; N, 14.49.

Synthesis of 1-FeSi. A toluene solution of 4-(trimethylsilyl)pyrazole (0.40 g, 2.85 mmol) was added dropwise at −78 °C to a solution of $FcBBr_2$ (0.34 g, 0.96 mmol) in 30 mL of toluene with efficient stirring. Neat NEt_3 (0.19 g, 1.88 mmol) was added, and the reaction mixture was warmed to ambient temperature and stirred for 12 h. After filtration from $HNEt_3Br$, the orange solution was added dropwise with stirring at ambient temperature to a slurry of $FeCl_2$ (0.08 g, 0.63 mmol) and NEt_3 (0.10 g, 0.99 mmol) in 15 mL of THF. A clear red solution was obtained, and after some time, a white precipitate formed ($HNEt_3Cl$). The slurry was stirred for another 2 h and filtered, and the filtrate was evaporated under reduced pressure. The residue was extracted into 20 mL of toluene, hexane was added (20 mL), all insolubles were removed by filtration, and the filtrate was concentrated slowly in vacuo. An amber microcrystalline solid was obtained, which was treated with 30 mL of hexane, collected on a frit, and dried in vacuo. Yield: 0.43 g (70%).

^{11}B NMR (128.3 MHz, $CDCl_3$): δ −0.6 ($h_{1/2}$ = 200 Hz). ^{1}H NMR (400.0 MHz, $CDCl_3$): δ 0.06 (s, 54H, $SiMe_3$), 4.34 (s, 10H, C_5H_5), 4.63, 4.66 (2 × br, 2 × 4H, C_5H_4), 6.7, 8.2 (2 × very br, 2 × 6H, pz-H3,5). ^{13}C NMR (100.5 MHz, [D_8]toluene, +80 °C): δ 0.2 ($SiMe_3$), 69.4 (C_5H_5), 70.9, 75.5 (C_5H_4), n.o. (C_5H_4-*ipso*), 117.0 (pz-C4), 145.8, 156.6 (pz-C3,5). FAB-MS: *m/z* 1282 [(M^+)]. Anal. Calcd for $C_{56}H_{84}B_2Fe_3N_{12}Si_6$ (1282.39): C, 52.45; H, 6.55; Fe, 13.07; N, 13.11. Found: C, 52.47; H, 6.68; Fe, 12.78; N, 13.37.

Synthesis of 1-MoLi. A mixture of **1-Li** (1.22 g, 3.02 mmol) and $Mo(CO)_6$ (1.21 g, 4.58 mmol) in 60 mL of acetonitrile was refluxed until gas evolution (CO) ceased (ca. 5 h). A small amount of brown precipitate was removed by filtration and the orange filtrate evaporated to dryness. The residue was treated three times with 15 mL of toluene to remove impurities, whereupon **1-MoLi** was obtained as a yellow microcrystalline solid. Yield: 1.62 (83%).

IR (CH_3CN): ν(CO) = 1758, 1892 cm^{-1}. ^{11}B NMR (128.3 MHz, CD_3CN): δ −0.8 ($h_{1/2}$ = 150 Hz). ^{7}Li NMR (155.4 MHz, CD_3CN): δ −2.4. ^{1}H NMR (400 MHz, CD_3CN, −30 °C): δ 4.23 (s, 5H, C_5H_5), 4.31, 4.54 (2 × vtr, 2 × 2H, J(HH) = 1.8 Hz, C_5H_4), 5.87 (vtr, 1H, J(HH) = 1.8 Hz, pz-H4a), 6.19 (vtr, 2H, J(HH) = 1.8 Hz, pz-H4b), 6.40, 7.65 (2 × d, 2 × 1H, J(HH) = 1.8 Hz, pz-H3,5a), 7.75, 8.70 (2 × d, 2 × 2H, J(HH) = 1.8 Hz, pz-H3,5b). ^{13}C NMR (100.5 MHz, CD_3CN): δ 69.9 (C_5H_5), 71.3, 76.0 (C_5H_4), n.o. (C_5H_4-*ipso*), 104.8 (pz-C4), 135.7, 144.1 (pz-C3,5), 231.8 (CO). Anal. Calcd for $C_{22}H_{18}BFeLiMoN_6O_3$·1.5$CH_3CN$ (583.84 + 41.02): C, 46.52; H, 3.49; Li, 1.1; Mo, 14.87; N, 16.28. Found: C, 46.17; H, 3.78; Li, 0.9; Mo, 14.43; N, 15.89.

Synthesis of 1-Mo. The entire yield of **1-MoLi** (1.62 g, 2.51 mmol) was dissolved in 40 mL of acetonitrile, neat 3-bromo-2-methyl-1-propene (0.81 g, 6.00 mmol) was added at ambient temperature, and the mixture was refluxed for 12 h. The solvent was removed in vacuo and the residue treated with hexane (30 mL); the insoluble crude product was collected on a frit and recrystallized from toluene/acetonitrile to give yellow X-ray-quality crystals. Yield: 1.39 g (92%).

IR (CH_2Cl_2): ν(CO) = 1847 (s), 1941 (vs) cm^{-1}. ^{11}B NMR (128.3 MHz, $CDCl_3$): δ −1.3 ($h_{1/2}$ = 150 Hz). ^{1}H NMR (400 MHz, [D_8]toluene, +80 °C): δ 1.31 (br, 2H, =CH*H*), 1.39 (s, 3H, CH_3), 3.26 (br, 2H, =C*H*H), 3.88 (s, 5H, C_5H_5), 4.01, 4.19 (2 × vtr, 2 × 2H, J(HH) = 1.8 Hz, C_5H_4), 5.8 (br, 3H, pz-H4), 7.8, 7.9 (2 × br, 2 × 3H, pz-H3,5). ^{1}H NMR (400 MHz, [D_8]toluene, −70 °C): δ 1.35, 1.38 (br, 2 × 1H, =CH*H*), 1.38 (s, 3H, CH_3), 3.19, 3.24 (br, 2 × 1H, =C*H*H), 3.76 (s, 5H, C_5H_5), 3.81, 3.90, 4.02, 4.04 (br, 4 × 1H, C_5H_4), 5.48 (vtr, 1H, J(HH) = 1.8 Hz, pz-H4a), 5.73 (vtr, 1H, J(HH) = 1.8 Hz, pz-H4b), 5.89 (vtr, 1H, J(HH) = 1.8 Hz, pz-H4b′), 6.63 (d, 1H, J(HH) = 1.8 Hz, pz-H5a), 7.21 (d, 1H, J(HH) = 1.8 Hz, pz-H3b), 7.47 (d, 1H, J(HH) = 1.8 Hz, pz-H3b′), 8.20 (d, 1H, J(HH) = 1.8 Hz, pz-H5b), 8.50 (d, 1H, J(HH) = 1.8 Hz, pz-H3a), 8.61 (d, 1H, J(HH) = 1.8 Hz, pz-H5b′). ^{13}C NMR (100.5 MHz, [D_8]toluene, +80 °C): δ 18.4 (CH_3), 59.4 (=CH_2), 69.5 (C_5H_5), 70.9, 75.6 (C_5H_4), n.o. (C_5H_4-*ipso*), 83.5 (*C*CH_3), 104.8 (pz-C4), 135, 145 (2 × br, pz-C3,5), 227.9 (CO). CI-MS: [*m/z* (%)]: 606 [(M^-); 100%], 578 [(M^- − CO); 4%]. Anal. Calcd for $C_{25}H_{25}BFeMoN_6O_2$ (604.11): C, 49.70; H, 4.14; Mo, 15.88; N, 13.91. Found: C, 49.73; H, 4.21; Mo, 15.97; N, 13.80.

Synthesis of 2-MoLi. A mixture of **2-Li**·0.7THF (0.62 g, 0.92 mmol) and $Mo(CO)_6$ (0.61 g, 2.31 mmol) in 50 mL of acetonitrile was refluxed until gas evolution (CO) ceased (ca. 5 h). A small amount of brown precipitate was removed by filtration, and the orange filtrate was evaporated in vacuo. The residue was treated three times with 20 mL of toluene to remove impurities, whereupon insoluble **2-MoLi** was obtained as a yellow microcrystalline solid. Yield: 0.73 g (78%).

IR (CH_3CN): ν(CO) = 1759 (s), 1892 (s) cm^{-1}. ^{11}B NMR (128.3 MHz, CD_3CN): δ 0.5 ($h_{1/2}$ = 200 Hz). ^{7}Li NMR (155.4 MHz, CD_3CN): δ −1.5. ^{1}H NMR (400.0 MHz, CD_3CN): δ 4.49, 4.54 (2 × vtr, 2 × 4H, J(HH) = 1.8 Hz, C_5H_4), 5.90 (br, 2H, pz-H4a), 6.24 (br, 4H, pz-H4b), 6.47, 7.70 (2 × br, 2 × 2H, pz-H3,5a), 7.80, 8.82 (2 × br, 2 × 4H, pz-H3,5b). ^{13}C NMR (100.5 MHz, CD_3CN): δ 73.1, 76.8 (C_5H_4), n.o. (C_5H_4-*ipso*), 105.2 (br, pz-C4a), 105.2 (br, pz-C4b), 135.4 (br, pz-C3,5b), 136.0 (br, pz-C3,5a), 144.3 (br, pz-C3,5a,b), 231.4, 232.0 (br, CO). Anal. Calcd for $C_{34}H_{26}B_2FeLi_2Mo_2N_{12}O_6$·$CH_3CN$ (981.69 + 41.02): C, 42.28; H, 2.84; Li, 1.3; Mo, 18.76; N, 17.81. Found: C, 41.94; H, 3.18; Li, 1.1; Mo, 18.25; N, 17.66.

Synthesis of 2-Mo. The entire yield of **2-MoLi** (0.73 g, 0.71 mmol) was dissolved in 40 mL of acetonitrile, neat 3-bromo-2-methyl-1-propene (0.37 g, 2.74 mmol) was added at ambient temperature, and the mixture was refluxed for 12 h. Subsequently, all volatiles were removed in vacuo, and the residue was treated with hexane (30 mL). The insoluble crude product was collected on a frit and recrystallized from toluene/hexane to give yellow crystals of **2-Mo**. Yield: 0.47 g (65%).

IR (CH_2Cl_2): ν(CO) = 1849 (s), 1942 (vs) cm^{-1}. ^{11}B NMR (128.3 MHz, $CDCl_3$): δ −1.0 ($h_{1/2}$ = 300 Hz). ^{1}H NMR (400.0 MHz, [D_8]toluene, + 80 °C): δ 1.33 (br, 4H, =CH*H*), 1.43 (s, 6H, CH_3), 3.27 (br, 4H, =C*H*H), 4.08, 4.11 (2 × br, 2 × 4H, C_5H_4), 5.83 (br, 6H, pz-H4), 7.9 (very br, br, 2 × 6H, pz-H3,5). ^{1}H NMR (400 MHz, [D_8]toluene, −70 °C): δ 1.37, 1.39 (2 × br, 2 × 2H, =CH*H*), 1.45 (s, 6H, CH_3), 3.22, 3.26 (2 × br, 2 × 2H, =C*H*H), 3.66, 3.76, 3.78, 3.80, 3.82, 3.84, 3.87, 3.94 (8 × br, 8 × 1H, C_5H_4), 5.43, 5.79, 5.92 (3 × br, 3 × 2H, pz-H4), 6.44, 7.22, 7.48 (3 × br, 3 × 2H, pz-H3,5), 8.14, 8.49, 8.52 (3 × br, 3 × 2H, pz-H3,5). ^{13}C NMR (100.5 MHz, [D_8]toluene, +80 °C): δ 18.5 (CH_3), 59.5 (=CH_2), 72.7, 76.5 (C_5H_4), n.o. (C_5H_4-*ipso*), 83.5 (*C*CH_3), 105.0 (pz-C4), 136, 145 (2 × br, pz-C3,5), 227.8 (CO). FAB-MS: *m/z* 966 [(M^+ − 2CO); 100%] , 854 [(M^+ − 4CO − H_2C=C(CH_3)-CH_3); 30%]. Anal. Calcd for $C_{40}H_{40}B_2$-

$FeMo_2N_{12}O_4 \cdot 1.5CH_3CN$ (1021.87 + 41.02): C, 47.67; H, 4.11; N, 17.46. Found: C, 47.83; H, 4.17; N, 17.36.

Reaction of 2-Li with $ZrCl_4$. Cold CH_2Cl_2 (50 mL; −78 °C) was added to a solid mixture of **2-Li** (0.96 g, 1.43 mmol) and $ZrCl_4$ (1.33 g, 5.71 mmol), and the resulting suspension was slowly warmed to ambient temperature and stirred for 12 h. Insoluble material was collected on a frit (G4) and extracted two times with 10 mL of CH_2Cl_2. The solvent was removed from the filtrates in vacuo, and a yellow solid residue was obtained. NMR spectroscopy showed it to contain several different products.

Reaction of 2-Li with $[Me_3O]BF_4$. Cold CH_2Cl_2 (20 mL; −78 °C) was added to a solid mixture of **2-Li**·0.7THF (0.21 g, 0.31 mmol) and $[Me_3O]BF_4$ (1.09 g, 0.61 mmol), and the resulting suspension was slowly warmed to ambient temperature and stirred for 12 h to give a yellow solution and a white precipitate. NMR spectroscopy showed the solution to contain a mixture of several components, with the *ansa*-ferrocenophane **D** as the main product (40%).[14]

Crystal Structure Determination of 1-Mo. A yellow crystal of **1-Mo** was selected in a perfluorinated oil and mounted in a glass capillary on an image plate diffraction system (IPDS, STOE). Final lattice parameters were obtained by least-squares refinement of 1935 reflections (graphite monochromator, λ = 0.710 73 Å, Mo Kα). Data: empirical formula $C_{25}H_{25}BFeMoN_6O_2$, M = 604.11, triclinic system, space group $P\bar{1}$ (No. 2); a = 8.756(1) Å, b = 12.154(1) Å, c = 12.927(1) Å, α = 105.26(1)°, β = 102.29(1)°, γ = 105.09(1)°, V = 1221.6(2) Å^3, crystal size 0.76 × 0.25 × 0.25 mm, D_{calc} = 1.642 g cm^{-3}, Z = 2. Data were collected at 223(±1) K, with a distance from crystal to image plate of 75 mm (1.5° < Θ < 25.1°), 360 images collected, 0° < φ < 360°, $\Delta\varphi$ = 1°, and exposure time 2 min. Data were corrected for Lorentz and polarization terms. A decay and absorption correction (μ = 11.4 cm^{-1}) was not applied; 15 167 data were measured, with 3926 independent reflections with $I > 0.01\sigma(I)$ used for refinement. The structure was solved by the Patterson method[31] and refined with standard difference Fourier techniques. All hydrogen atoms were located in difference Fourier maps and refined isotropically. Additional data: Number of parameters refined, 425; 9.2 data per parameter; weighting scheme $w = 1/[\sigma^2(F_o^2) + (0.0587P)^2 + 0.9786P]$, where $P = (F_o^2 + 2F_c^2)/3$; shift/error <0.001 in the last cycle of refinement; residual electron density +0.36 e Å^{-3}, −0.56 e Å^{-3}; $R1$ = 0.031, w$R2$ = 0.088; minimized function was $\Sigma w(F_o^2 - F_c^2)^2$.

Electrochemistry. The materials and apparatus for electrochemistry have been described elsewhere.[30] All the potential values are referred to the saturated calomel electrode (SCE).

Acknowledgment. We are grateful to Prof. Dr. W. A. Herrmann (Technische Universität München) for his generous support. M.W. thanks the "Deutsche Forschungsgemeinschaft", and the "Fonds der Chemischen Industrie" for financial funding. P.Z. gratefully acknowledges the financial support by MURST of Italy (quota 60%).

Supporting Information Available: An X-ray crystallographic file in CIF format for complex **1-Mo** is available on the Internet only. Access information is given on any current masthead page.

IC9612360

(31) Sheldrick, G. M. *Acta Crystallogr., Sect. A* **1990**, *46*, 457−473.